2023-11-17

Facile biosynthesis of Ag–ZnO nanocomposites using Launaea cornuta leaf extract and their antimicrobial activity

Makauki, Elizabeth

Springer Nature

https://doi.org/10.1186/s11671-023-03925-2

Discover Nano

Discover

Research

Facile biosynthesis of Ag–ZnO nanocomposites using *Launaea cornuta* leaf extract and their antimicrobial activity

Elizabeth Makauki[1] · Stanslaus George Mtavangu[2,4] · Onita D. Basu[3] · Mwemezi Rwiza[1] · Revocatus Machunda[1]

Received: 14 August 2023 / Accepted: 14 November 2023
Published online: 17 November 2023

Abstract
The quest to synthesize safe, non-hazardous Ag–ZnO nanoomposites (NCs) with improved physical and chemical properties has necessitated green synthesis approaches. In this research, *Launaea cornuta* leaf extract was proposed for the green synthesis of Ag–ZnO NCs, wherein the leaf extract was used as a reducing and capping agent. The antibacterial activity of the prepared nanoomposites was investigated against *Escherichia coli* and *Staphylococcus aureus* through the disc diffusion method. The influence of the synthesis temperature, pH, and precursor concentration on the synthesis of the Ag–ZnO NCs and antimicrobial efficacy were investigated. The nanoparticles were characterized by ATR-FTIR, XRD, UV–Vis, FESEM, and TEM. The FTIR results indicated the presence of secondary metabolites in *Launaea cornuta* which assisted the green synthesis of the nanoparticles. The XRD results confirmed the successful synthesis of crystalline Ag–ZnO NCs with an average particle size of 21.51 nm. The SEM and TEM images indicated the synthesized nanoparticles to be spherical in shape. The optimum synthesis conditions for Ag–ZnO NCs were at 70 °C, pH of 7, and 8% silver. Antibacterial activity results show Ag–ZnO NCs to have higher microbial inhibition on *E. coli* than on *S. aureus* with the zones of inhibition of 21 ± 1.08 and 19.67 ± 0.47 mm, respectively. Therefore, the results suggest that *Launaea cornuta* leaf extract can be used for the synthesis of Ag–ZnO NCs.

Keywords Green synthesis · *Launaea cornuta* · Metabolites · Nanoparticles · Microbial growth inhibition

1 Introduction

During the last decade research in metal and metal oxide nanomaterials has gained popularity due to their distinctive properties and potential applications in various environmental and health fields. Metal and metal oxide nanomaterials are characterized by their small size (1–100 nm) and shape which results in a higher surface area-to-volume ratio influencing and improving the optical, catalytic, electrical, magnetic, and conductive properties of these materials [1–4]. Silver nanoparticles (Ag NPs), in particular, stand out amongst metal nanoparticles and their bulk counterparts due to their remarkable features and high activity potential which has led to significant advancements in several fields including pharmaceuticals, agriculture, biosensors, and water treatment [5, 6]. These nanoparticles exhibit exceptional resistance

Supplementary Information The online version contains supplementary material available at https://doi.org/10.1186/s11671-023-03925-2.

✉ Elizabeth Makauki, elizabeth.makauki@nm-aist.ac.tz | [1]School of Materials Energy Water and Environmental Sciences, Nelson Mandela African Institution of Science and Technology, Arusha, Tanzania. [2]Department of Chemical Engineering, Faculty of Engineering Sciences, KU Leuven, Leuven, Belgium. [3]Department of Civil and Environmental Engineering, Faculty of Engineering and Design, Carleton University, Ottawa, Canada. [4]Department of Chemistry, Dar es Salaam University College of Education, Dar es Salaam, Tanzania.

against microorganisms, making them potent biocidal agents against both gram-positive and gram-negative bacteria. Notably, Ag NPs possess high thermal stability, low volatility and toxicity towards mammalian cells making them preferred in health-related applications [7]. Leveraging their antimicrobial properties, Ag NPs are extensively used in controlled and targeted drug delivery systems, capitalizing on their low toxicity and biocompatibility [8]. Furthermore, their high surface plasmon resonance makes them ideal candidates for the development of biosensors, showcasing their versatility and potential for scientific and technological innovations [3, 9–11]. Despite their great capacity for microbial growth inhibition, the reactive nature of Ag NPs associated with high inter-particle attraction and surface forces consequently results in agglomeration which leads to a reduction of the Ag NPs antimicrobial properties [12–14]. To prevent agglomeration and thereby maintain effective microbial inhibition, Ag NPs may be doped into semiconductor-based heterostructures, such as ZnO therefore making the nanoparticles multifunctional [11, 15–17]. The agglomeration and particle size are controlled as the Ag NPs are attached in the ZnO structure, therefore, reducing self-inter-particle attraction [13]. Shreema et al. [18] observed decreased agglomeration and complete separation of particles on the doping of pure ZnO.

Zinc oxide (ZnO) is a metal oxide semiconductor with a direct wide band gap (3.37 eV). It is an attractive photocatalyst owing to its high photosensitivity, high thermal stability and environmental sustainability [19–22]. Furthermore, ZnO nanoparticles exhibit significant antibacterial efficacy against both gram-positive and gram-negative bacteria even in the absence of light, highlighting their immense potential in combating microbial infections [23]. Doping of metallic elements into ZnO is reported to improve its antimicrobial efficiency as it increases the electron–hole (e–h) separation efficiency therefore enhances photocatalytic activity [16, 24]. Silver-doped zinc oxide nanocomposites, (Ag–ZnO NCs) have been reported to be more effective against gram-positive and gram-negative bacteria, compared to pure ZnO [13, 25]. The association of Ag and ZnO nanoparticles increases the formation of reactive oxygen species (ROS) leading to increased antimicrobial activity [26].

In addition, the agglomeration of silver nanoparticles can be controlled through the use of chemical stabilizing agents such as polyvinylpyrrolidone (PVP), polyvinylalcohol (PVA), hyperbranchedpolyurethane (HP), and polyacrylonitrile (PAN) [27, 28]. Chemical methods include flow—injection, co-precipitation, sol–gel synthesis, micro-emulsion, and hydrothermal reactions [29, 30]. However chemically synthesized nanoparticles have been reported to release toxins at nanoscale and have been linked with elevated causes of diseases such as cancer [5, 31–33]. Chemically synthesized nanoparticles, therefore, may threaten environmental sustainability and limits the human consumption-related applications of these noble materials. Furthermore, physical methods to control agglomeration involve milling, thermal ablation, and grinding but have reported extremely low yields compared to the energy applied [34, 35].

Due to these challenges, there is a need to incorporate the "green chemistry," technology, an idea that encourages the replacement of conventional chemicals with the non-toxic, and environmentally friendly reducing agents [36–40]. Green synthesis of nanoparticles includes the use of active ingredients from bacteria, fungi, and plants as reducing and stabilizing agents [19, 41, 42]. Plant extracts have been used and greatly influenced the properties of the synthesized nanoparticles depending on the type and quantity of bioactive materials present in the specific plant [43–45]. Plant extracts are deemed to be beneficial than conventional chemicals taking into consideration of their easy accessibility, biodegradability and minimal harmful effects [46]. Yet, limited plant species have had their efficacy in green synthesis validated scientifically. Plant extracts have secondary metabolites such as flavonoids, alkaloids, tannins, proteins, polyphenols, terpenoids, and saponins [1, 14, 47, 48]. Alkaloids, tannins, proteins, polyphenols, and terpenoids act as hydrolyzing/reducing agents reducing metal ions into atoms [28, 49, 50]. The plant's flavonoids and saponins act as capping/stabilizing agents, controlling the size and agglomeration of the nanoparticles during synthesis [51, 52]. As a result, green synthesis becomes a basis for the effective evaluation and development of non-toxic nanomaterials used in drug formulations, water treatment and environmental remediation with limited side effects[35].

As far as we are aware, there is no study that has documented the use of *Launaea cornuta* leaf extract for synthesizing Ag-ZnO NCs. This research therefore explores the novel potential of *Launaea cornuta* leaf extract in green synthesis of Ag-ZnO NCs from nitrates of Ag and Zinc. *Launaea cornuta* belongs to the wild lettuce family; it is used as a vaso-relaxant, sedative, cough suppressant, expectorant and antiseptic [53, 54]. The root is used in the treatment of gonorrhoea, syphilis, sore throat, cough, and eye infections [55]. Traditionally, *Launaea cornuta* has been used to alleviate inflammatory conditions such as joint pains, earaches and swollen testicles [56]. This plant is known to contain significant amounts of ascorbic acid (vitamin C), phenols, tannins, alkaloids, and flavonoids compounds essential in green synthesis as reducing and capping agents [56–58]. The study further investigates the influence of synthesis temperature, pH of media, and silver dopant concentrations on the synthesized NPs. The antimicrobial efficiency of the synthesized NPs is tested against gram-positive (*Staphylococcus aureus*) and gram-negative (*Escherichia coli*) bacteria.

2 Materials and methods

2.1 Materials

Launaea cornuta leaves were collected randomly from the fields of the Nelson Mandela African Institution of Science and technology, Nambala village in Arusha region, Tanzania wat 3° 23′ 58″ S 36° 47′ 48″ E coordinates. The plant was identified and deposited at National Herbarium of Tanzania (NHT) at the Tanzania Plant Health and pesticides Authority (TPHPA) with reference no. KA51/2023. The collection of the plant materials adhered to applicable institutional, national, and international laws and guidelines.

$AgNO_3$ (99.99%), hydrous $Zn(NO_3)_2$ (99.99%), NaOH (98%), Ciprofloxacin (98%) and ethanol (99.5%) used in this experiment were purchased from Sigma-Aldrich Chemicals (Germany) and were used without any further purification. The solutions of these analytical precursors were prepared by double distilled water. *Staphylococcus aureus* (ATCC 25923) and *Escherichia coli* (ATCC 25922) bacterial strains were obtained from the laboratory of The Nelson Mandela African Institution of Science and Technology (NM-AIST) Arusha Tanzania.

2.2 Methods

2.2.1 Preparation of *Launaea cornuta* leaf extract

The collected *Launaea cornuta* leaves were washed three times with double distilled water to remove sand and any other impurities. The washed leaves were left for 6 h to drain water used in the washing process. 100 g of the *Launaea cornuta* leaves were sliced into small pieces and mixed with 50 mL double distilled water then ground into a fine paste using an electric blender. The resulting paste was introduced into shaking on an electrical shaker for 24 h to allow maximum extraction of the secondary metabolites (phytochemical compounds) from the *Launaea cornuta* leaves. The paste was centrifuged for 20 min under 4000 rpm to separate the leaf extract from the leaf residues. The aqueous extract was further filtered using Whatman No. 1 filter paper to make sure all the leaf particles are removed from the extract. The final obtained *Launaea cornuta* leaf extract with a pH of 5.6 was stored at 4 °C, ready for the green synthesis of Ag-ZnO NCs.

2.2.2 Synthesis of Ag, ZnO nanoparticles and Ag-ZnO nanocomposite

2.2.2.1 Biosynthesis of Ag nanoparticles Ag NPs were synthesized based on the method reported in literature with some modifications [1]. $AgNO_3$ was dissolved in double distilled water to prepare a 0. 1 M $AgNO_3$ stock solution. 92 mL of *Launaea cornuta* leaf extract was added in a 150 mL beaker under vigorous stirring, 8 mL of 0.1 M $AgNO_3$ solution was added dropwise to the leaf extract to make a 8 mM solution. The flask was left to stir for 2 h at a 70 °C, pH was adjusted to 7 using 0.1 M NaOH. The resulting solution was centrifuged and the solid particles obtained were washed twice by 50% ethanol before oven drying for 12 h under 100 °C and then calcined at 650 °C for 3 h. The Ag NPs were stored in an air tight container ready for characterization and antimicrobial test.

2.2.2.2 Biosynthesis of ZnO nanoparticles Synthesis of ZnO NPs and Ag-ZnO NCs was adopted from Mtavangu et al. [25] with modifications. 92 mL of *Launaea cornuta* leaf extract was placed in a 150 mL beaker under vigorous stirring, 2.9748 g of $Zn(NO_3)_2.6H_2O$ salt was added to the leaf extract under stirring. The reaction was left to continue for 2 h under constant stirring at a 70 °C temperature and pH 7. The resulting solution was centrifuged, and the paste was washed twice by 50% ethanol before oven drying 12 h under 100 °C and then calcined at 650 °C for 3 h to obtain ZnONPs. The ZnONPs were stored in an air tight container ready for characterization and antimicrobial test.

2.2.2.3 Biosynthesis of Ag-ZnO nanocomposite 92 mL of *Launaea cornuta* leaf extract was placed in a 150 mL beaker under vigorous magnetic stirring, 8 mL of 0.1 M $AgNO_3$ solution was added dropwise to the leaf extract to make a 8 mM solution. After 20 min 2.97 g of $Zn(NO_3)_2$ salt was added and the pH was adjusted to 7 by using 0.1 M NaOH. The flask was wrapped with aluminum foil and the solution was left to stir for 2 h at a 70 °C temperature. The resulting Ag–ZnO solution was centrifuged, and the paste was washed twice by 50% ethanol before oven drying 12 h under 100 °C and then calcined under 650 °C for 3 h to get Ag–ZnO NCs. The Ag–ZnO NCs were stored in a dry container ready for characterization and antimicrobial test. The reaction was repeated by altering the reaction temperature (30, 50, 70, and 90 °C),

different pH (5, 7, 9 and 11, and 13), and different Ag^+ concentrations (4, 6, 8, and 10 mM) to identify optimum synthesis conditions.

2.2.2.4 Material characterization The crystalline nature of synthesized nanomaterials was analysed using Rebaku Smart-Lab X-ray diffractometer (XRD) equipped with analyser scanning mode of CuKα wavelength (λ) = 1.54059 Å, 40 kV–30 mA and 2θ/θ with the spectrum range between 30° and 80°, 0.02 step and 0.2 speed [25]. The identification of functional groups was accomplished through attenuated total reflection-Fourier transform infrared (ATR-FTIR) spectroscopy using the Bruker Optic GmbH 2011 (alpha model, Laser class 1) instrument operating in transmittance mode. Spectral analysis was conducted within the range of 4000–400 cm^{-1} with a spectral resolution of 2 cm^{-1}. The formation of silver nanoparticles (Ag NPs) and silver-zinc oxide nanocomposites (Ag–ZnO NCs) was assessed by recording the ultraviolet–visible (UV–Vis) absorption spectra using a UVmini-1240 Shimadzu spectrophotometer from 250 to 800 nm. The particle size, shape, and morphology of the synthesized nanoparticles were characterized by high-resolution transmission electron microscopy—HR-TEM (JEOL JEM 2100, 80–200 kV, Jeol Ltd. Japan) and Field emission scanning electron microscopy (FE-SEM) while the elemental composition was characterized by EDX.

2.2.2.5 Antimicrobial assay The antimicrobial efficacy of the produced silver nanoparticles (Ag NPs), zinc oxide nanoparticles (ZnO NPs), and silver-zinc oxide nanocomposites (Ag–ZnO NCs) was evaluated against gram-positive (*Staphylococcus aureus*-ATCC 25923) and gram-negative (*Escherichia coli*-ATCC 25922) bacterial strains using the disc diffusion method [15]. Sterilized nutrient agar media was poured into sterilized Petri dishes and allowed to solidify. Upon solidification, individual agar plates were inoculated with each bacterial strain and uniformly spread using a sterilized swab. Absorbent discs, 6 mm in diameter and sterilized, were immersed in colloidal solutions of Ag NPs, ZnO NPs, and Ag–ZnO NCs with concentrations ranging from 10 to 50 mg/mL. These soaked discs were then placed on the inoculated Petri dishes. After 24 h of incubation at 37 °C, the bacterial inhibition results were interpreted and presented in terms of the zone of inhibition (ZOI) and minimum inhibition concentration (MIC) in millimeters. Ciprofloxacin served as the positive control in this study. Additionally, the antimicrobial activity of *Launaea cornuta* leaf extract (LE) was assessed since it is traditionally used in medicine.

3 Results and discussion

3.1 X-ray diffraction

Figure 1 diffractogram shows the XRD patterns of pure Ag NPs, ZnO NPs, and the Ag–ZnO NCs. It shows the Ag–ZnO NCs patterns with different Ag^+ content, synthesis temperature, and pH. The pure Ag NPs pattern indicated in Fig. 1a shows four strong peaks at 2θ values of 38.10, 44.28, 64.44, and 77.38 degrees which correspond to the crystal planes of (111), (200), (220), and (311). These patterns confirm the face-centered-cubic (fcc) crystalline nature of the synthesized AgNPs with lattice parameters a = b = c = 4.088 A° as compared to the silver standard powder diffraction card, JCPDS, file No. 04-0783 [59, 60]. The pure ZnO XRD patterns display eight diffraction peaks at 2θ values of 31.74°, 34.38°, 36.18°, 47.42°, 56.48°, 62.80°, 67.84°, and 68.24° corresponding to the crystal planes (100), (002), (101), (102), (110), (103), (112), and (201). The crystal planes matched well with the ZnO standard powder diffraction card JCPDS, File No. 01-076-0704 indicating the formation of the typical hexagonal wurtzite structure space group P 63 mc ZnO NPs in the matrix [24, 61]. Furthermore, the XRD pattern of the Ag–ZnO NCs exhibits the peaks that correspond to both Ag and ZnO, proof that Ag–ZnO NCs have been synthesized. These patterns are indications of peaks appeared at 2θ values of 31.74°, 34.38°, 36.18°, 38.10°, 44.28°, 47.42°, 56.48°, 62.80°, 64.44°, 67.84°, 68.24° and 77.38° corresponding to the crystal planes (100), (002), (101), (111), (200), (102), (110), (103), (220), (112), (201) and (311). The intensity of the Ag NPs peaks decreased in the composite as a result of successful doping by ZnO forming a core around the Ag NPs [62]. Figure 1b shows the effect of temperature in the synthesized Ag–ZnO NCs especially on the peaks representing the presence Ag NPs in the composite. The increase in synthesis temperature has led to an increase in intensity of peaks: (111), (200), (220), and (311). This suggests the formation of Ag NPs at high temperatures. This is attributed to the increased collision of the reacting species leading to the formation of more nuclei [41]. Figure 1c shows the effect of the reaction materials concentration. In this study, the concentration of the Ag^+ used was varied to evaluate its effect. It has been observed that as the Ag concentration increases the peak intensity increases. At low concentrations, the Ag NPs peaks were almost invisible. It might be contributed to being overshadowed by the

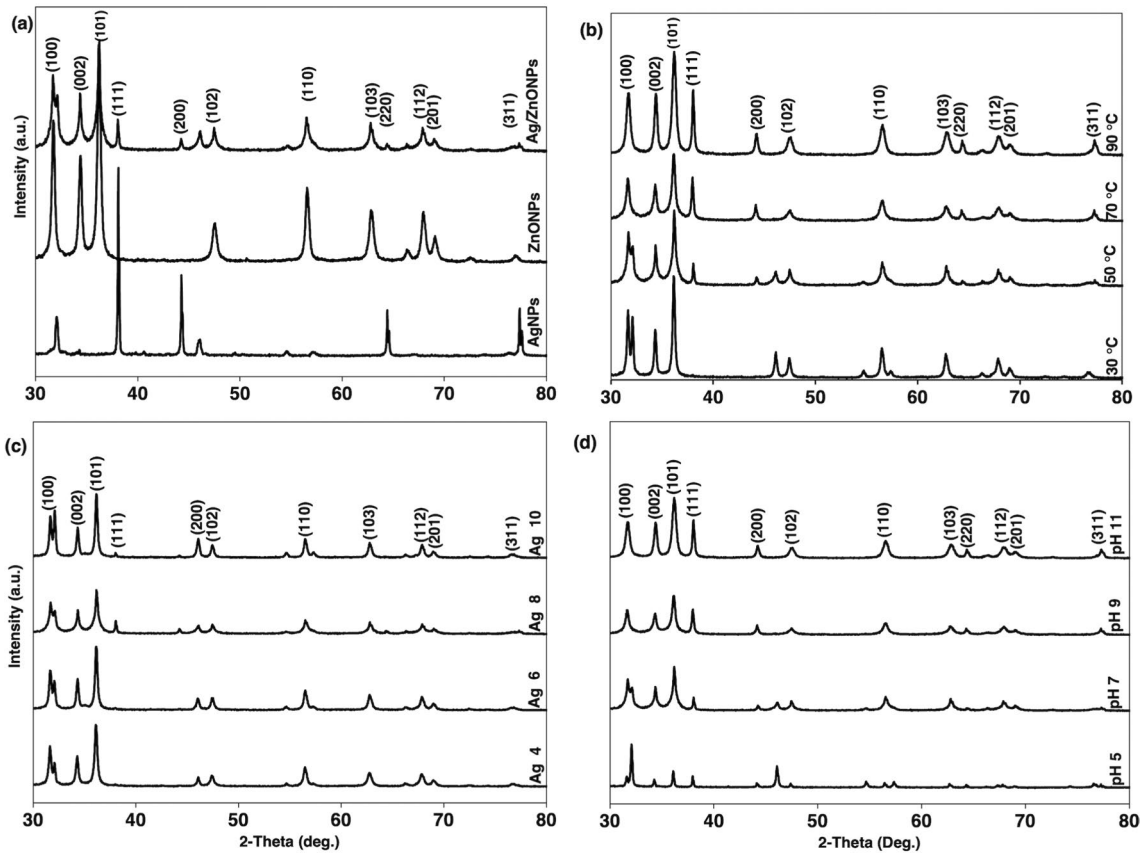

Fig. 1 XRD patterns of **a** pure Ag NPs, ZnO NPs and Ag–ZnO NCs, **b** Ag–ZnO NCs at different temperature, **c** Ag–ZnO NCs at different Ag^+ concentration and **d** Ag–ZnO NCs at different pH

ZnO NPs which surrounded the Ag NPs. Figure 1d shows the increased intensity of the composite peaks as the pH of the reacting solution changed from acidic to alkaline. This provides insight into the formation of more crystalline particles at around neutral to alkaline conditions during the synthesis process.

For the precise calculation of the average particle size of the synthesized materials the Debye–Scherrer equation represented by Eq. (1) was used where, K is the Scherrer constant (0.94), λ is the specific wavelength of the X-ray used which is 0.154 nm, β is the full width at half maxima, θ is the diffraction Bragg angle and D is the average crystallite size in nm.

$$D = \frac{K\lambda}{\beta_{2\theta}\cos\theta} \tag{1}$$

From this equation, the average crystallite size for pure Ag NPs, ZnO NPs, and Ag–ZnO NCs were 50.6, 22.1 and 21.5 nm respectively. Ag doping on ZnO has caused a subsequent decrease in the average crystal size of Ag which might be attributed to the dispersion of ZnO nanoparticles around the Ag lattice, which limits the coalition of Ag NPs, thus hindering its agglomeration. The average particle size decreased as the temperature increased, with values of 35.1 nm at 30 °C, 30.6 nm at 50 °C, and 21.5 nm at 70 °C. The increase in the reaction temperature leads to an increase in the reduction rate of the Zn^{2+} and Ag^+ ions. It also increases the subsequent homogeneous nucleation of ions causing the formation of small-size Ag–ZnO NCs [41, 63]. The particle size for the composites synthesized at pH 5, 7, 9, and 11 was 43.3, 21.5, 22.1 and 24.3 indicating the smallest particles to be obtained at the neutral pH [42, 64]. The Ag–ZnO NCs synthesized at 4, 6, 8, and 10% Ag had the average particle sizes 29.3, 26.8, 21.5 and 28.8 nm, respectively. Similar results reported were elsewhere [25].

3.2 Optical properties

3.2.1 ART-FTIR studies

FTIR spectrum of the *Launaea cornuta* leaf extract indicates the presence of alkaloids, saponins, flavonoids, and tannins as secondary metabolites responsible for reducing and capping of metal ions and nanoparticles respectively. Figure 2 indicates that FTIR spectra of *Launaea cornuta* leaf extract exhibited the peaks at a wavenumber 635 cm^{-1} which is attributed to the N–H stretching vibrations. The 1315 and 1006 cm^{-1} are attributed to the C–N stretching vibrations of the aromatic and aliphatic amines, respectively [65]. The presence of N–H and C–N peaks signifies the presence of aliphatic amine groups which confirms the presence of alkaloids [66, 67] which act as hydrolyzing/reducing agents in the formation of nanoparticles and nanocomposites. The strong and broad band at 3292 cm^{-1} indicates O–H and N–H stretching vibration [68] while the band at 1315 cm^{-1} indicates C–C starching [67]. These bands indicate the presence of flavonoids and tannins [51, 69]. The 1612 and 2922 cm^{-1} bands correspond to the C=C and C–H vibrations which indicates the presence of saponins in the leaf extract. The saponins, flavonoids, and tannins act as natural surfactants and capping agents controlling particle size growth and preventing agglomeration by providing a steric hindrance on the nanoparticles formed [70]. The shortening and disappearance of the O–H vibration observed after the biosynthesized Ag and Ag–ZnO NCs respectively may be due to the binding of the -OH on the surface of the nanoparticles and volatilization during calcination [51, 71]. The FTIR of the synthesized Ag NPs indicates a shortening of the 3292 cm^{-1} band, disappearing of 1315 and 635 cm^{-1} band as well as a shift of other bands from 2922 to 2975 cm^{-1}, 1612 to 1632 cm^{-1}, and 1006 to 1044 cm^{-1}. In the case of Ag–ZnO NCs there is a disappearance of the 3292, 2922, 1315, and 1612 cm^{-1} bands with a shift from 1006 to 1022 cm^{-1} and 635 to 577 cm^{-1} bands. These changes suggest the binding of the Ag and ZnO on the proteins through the free amine groups, hydroxyl and carboxylate ions of amino acid [41, 72]. The 6 cm^{-1} stretching peak indicates the presence of the synthesized ZnO in the biosynthesis process [73, 74].

3.2.2 UV–Vis spectrum

The aqueous leaf extract of *Launaea cornuta* was used for the green synthesis in this study. During the synthesis process the leaf extract color changed from light brown to brown after 10 min of addition of $AgNO_3$ solution becoming dark brown on addition of $Zn(NO_3)_2$ This is an initial indication of the formation of Ag NPs and ZnO NPs in the solution [75, 76]. The color change is a result of the excitation of the surface plasmon vibrations in the Ag NPs which causes color change in the solution [12, 14, 71, 75]. The UV–Vis spectrometry as illustrated in Fig. 3 depicts the absorption band peak at 403 nm providing evidence of the formation of Ag NPs [47, 77]. The addition of $Zn(NO_3)_2$ to form Ag–ZnO NCs, shifted the absorption band peaks to around 372 and 394 nm as the concentration of silver increased from 4 to 10%. This is the

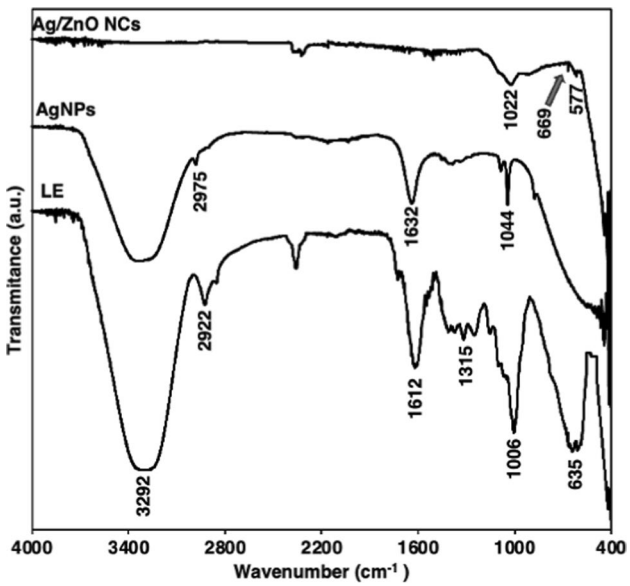

Fig. 2 FTIR patterns of leaf extract, Ag NPs and Ag–ZnO NCs

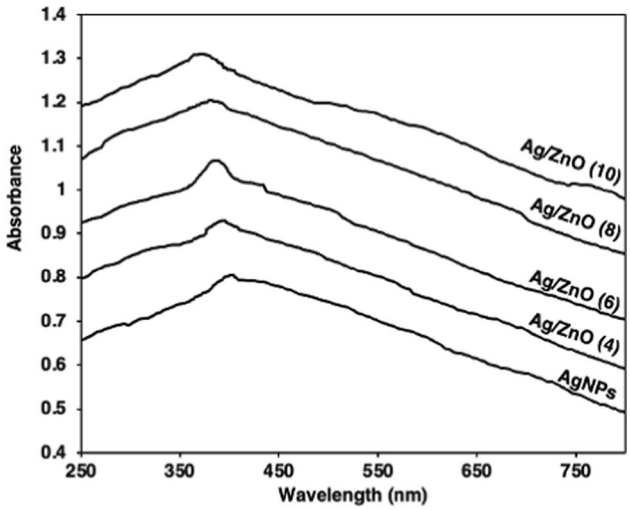

Fig. 3 UV–Vis patterns of Ag NPs and Ag–ZnO NCs in 4, 6, 8, and 10% Ag^{+}

evidence of the presence of ZnO on the prepared nanomaterials [17, 78]. In the investigation of the effect of doping concentration, 4, 6, 8, and 10% Ag^{+} were applied. In these concentrations, adsorption peaks were observed at 394, 386, 381, 372 nm. The increase of $AgNO_3$ concentration resulted in the shift of the peaks from 403 to 372 nm which is referred to as blue shift. The blue shift is a result of the Ag NPs attachment around ZnO NPs leading to the formation of smaller nuclei on the ZnO surface therefore decreasing the nanoparticles size [25, 79].

3.3 Morphological studies

3.3.1 Field emission scanning electron microscopy (FE-SEM)

Figure 4 illustrate the morphology of the synthesized nanomaterials by using *Launaea cornuta* leaf extract at different $AgNO_3$ concentrations. The FE-SEM images show that $AgNO_3$ concentration had significant effects on the morphologies

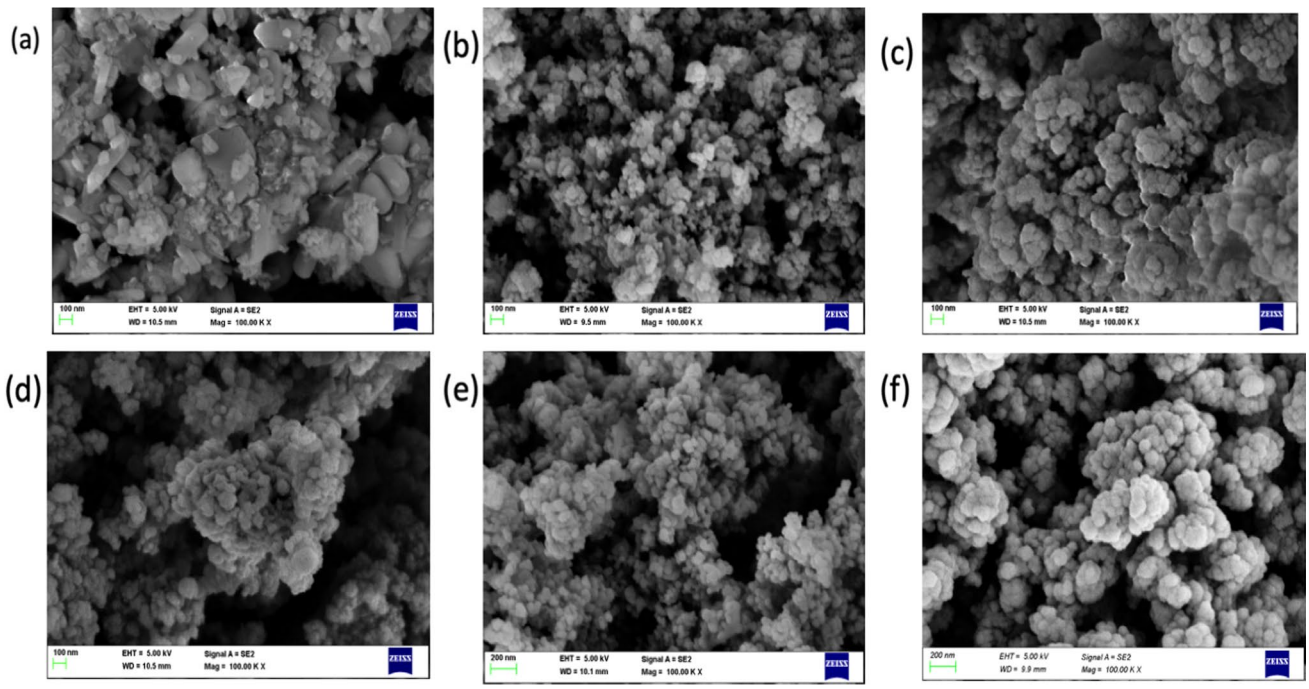

Fig. 4 SEM images of **a** pure Ag NPs, **b** pure ZnO NPs, and Ag–ZnO NCs with **c** 4%, **d** 6%, **e** 8% and **f** 10% Ag concentrations

of the synthesized nanoparticles [41, 42, 63, 64]. Ag NPs indicated in Fig. 4a were observed to have spherical, tubelike, and blocklike aggregated nanoparticles with an average particle size of 75.7 nm [63]. ZnO NPs in Fig. 4b displayed spherical agglomerated particles with an average particle size of 33.09 nm. Doping of the Ag NPs into ZnO had an effect on the shape and size of the resulting Ag–ZnO NCs composite. Ag-ZnO NCs demonstrated spherical agglomerated composites with the average particle size average of 36.11 nm. The decrease of particle size from pure Ag NPs to Ag–ZnO NCs might be attributed to the Ag NPs anchoring on the surface of ZnO NPs [80]. The average particle size for the composites synthesized at 30, 50, 70, and 90 °C were 46.75, 43.5, 36.11, and 39.29 nm respectively. As the temperature increased the particle size decreased, and the results correspond to the XRD results discussed above. The FE-SEM images, Fig. 4c–f, of the composites synthesized at concentrations 4, 6, 8, and 10% Ag^+ demonstrated particle size averages of 51.54, 50.16, 46.11, and 49 nm respectively decreasing as the Ag^+ percentage increases, a trend proved by the XRD results of this study. The smallest particle size was obtained at pH 7 condition. As the pH increases there is an increase in particle size caused by the increased nucleation that supports hydrolysis and accelerates the particle size growth due to agglomeration [81]. EDS spectra in Fig. 5 further proves the presence of Ag, Zn and O in the Ag–ZnO NCs synthesized samples. It is a proof that *Launaea cornuta* leaf extract can be used successfully to synthesiwe Ag–ZnO NCs.

3.3.2 High-resolution transmission electron microscopy (HR-TEM)

Figure 6a is the TEM of the Ag–ZnO NPs showing a dispersion of the spherical ZnO nanoparticles anchored on the surface of Ag nanoparticles which resulted to the controlled agglomeration of Ag NPs therefore decreased particle size. The particle size distribution of Ag–ZnO NCs ranges from 13.89 to 45.37 nm as illustrated in the histogram (inset in Fig. 6a) and its average particle size was 29.75 nm. The average particle size of Ag NPs and ZnO NPs were 59.78 and 26.5 nm respectively which corresponds to the result patterns of XRD and SEM. The addition of Ag NPs in the ZnO NPs matrix decreases the average particle size of Ag NPs by more than 50%. The selected area electron diffraction (SAED) pattern of Ag NPs, ZnO NPs and Ag–ZnO NCs indicate concentric rings as shown in Fig. 6b–d. The organized circular pattens explains the crystalline nature of prepared nanomaterials. The SAED pattern of Ag–ZnO NCs shows the increase of the cycles indicating the presence of both Ag and ZnO in the composite. The EDAX mapping of Ag–ZnO NCs indicated the composition and distribution of atoms present in the composite (Fig. 6e–h). The EDAX mapping demonstrates a consistent dispersion of Ag, Zn, and O within the composite material, confirming the successful incorporation of Ag into ZnO, as illustrated in Fig. 6e, f. These findings provide strong evidence that silver ions have been effectively integrated into the ZnO nanoparticles.

3.4 Antimicrobial assessment

Studies report a remarkable reduction in microbial growth when exposed to Ag NPs, ZnO NPs, and Ag–ZnO NCs [13, 77, 82–84]. In this study, antimicrobial activity of Ag NPs, ZnO NPs, and Ag/ZnO NCs against gram-negative (*E. coli*) and gram- positive (*S. aureus*) bacteria strains were examined. The effect of synthesis concentration, temperature, and pH

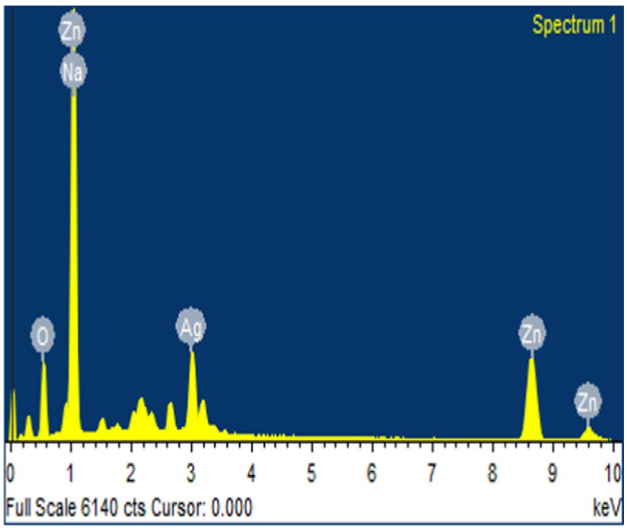

Fig. 5 EDS spectra of Ag–ZnO NCs

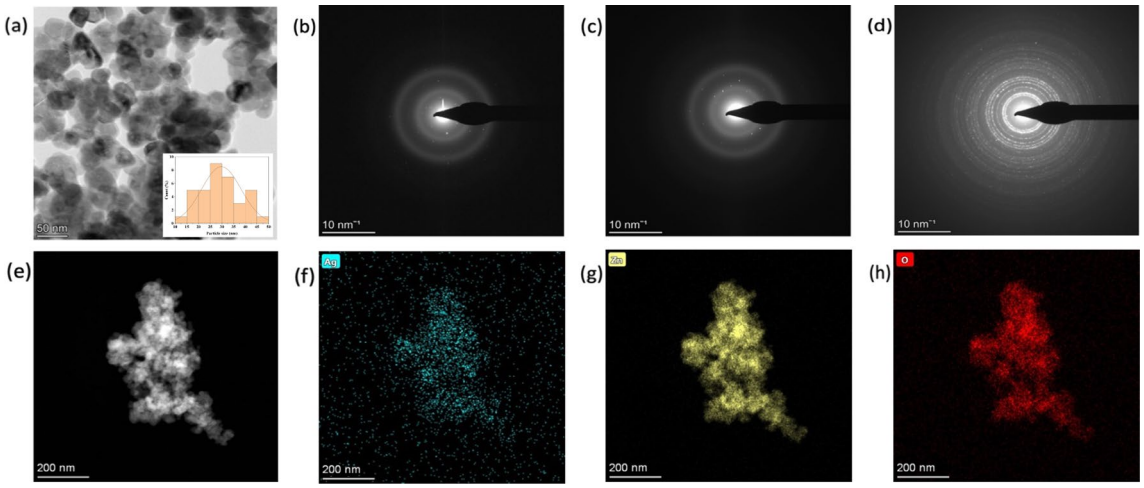

Fig. 6 **a** TEM of the Ag–ZnO NCs (the inset is particle distribution histogram), SAED patterns of **b** Ag NPs, **c** ZnO NPs, **d** Ag–ZnO NCs, and the EDAX mapping of **e** Ag–ZnO, **f** Ag, **g** Zn, and **h** O on the Ag–ZnO NCs

were investigated. Figure 7a indicates the ZOI for ciprofloxacin indicated as "control", *Launaea cornuta* leaf extract (LE) and the synthesized Ag NPs, ZnO NPs, and Ag-ZnO NCs. The existence of the zone of inhibition around the NPs indicates that the NPs are antimicrobial active. Ciprofloxacin exhibited an inhibition zone of 36.7 ± 1.2 and 34.7 ± 1.7 mm for *E. coli* and *S. aureus* respectively. The *Launaea cornuta* leaf extract (LE) was found to inhibit bacteria growth with the ZOI of 7.7 ± 0.5 and 7.3 ± 0.5 mm for *E. coli* and *S. aureus* respectively. As indicated in Fig. 7a Ag NPs have demonstrated the highest ZOI for both bacterial strains among the synthesized NPs followed by Ag–ZnO NCs and then ZnO NPs, as reported elsewhere [9, 85]. The highest ZOI of Ag NPs was 22.0 ± 0.8 mm and 20.2 ± 0.2 mm, for *E. coli* and *S. aureus* while that of Ag-ZnO NCs was 21 ± 1.1 mm and 19.7 ± 0.5 mm respectively. ZnO NPs had a ZOI of 11.0 ± 0.8 mm and 7.7 ± 0.9 mm, for *E. coli* and *S. aureus*. The *p* values for both strains were < 0.05 proving the significance of the results obtained. In this study, the *E. coli* (gram-negative) inhibition was higher than *S. aureus* (gram-positive) bacteria. This perspective is contributed

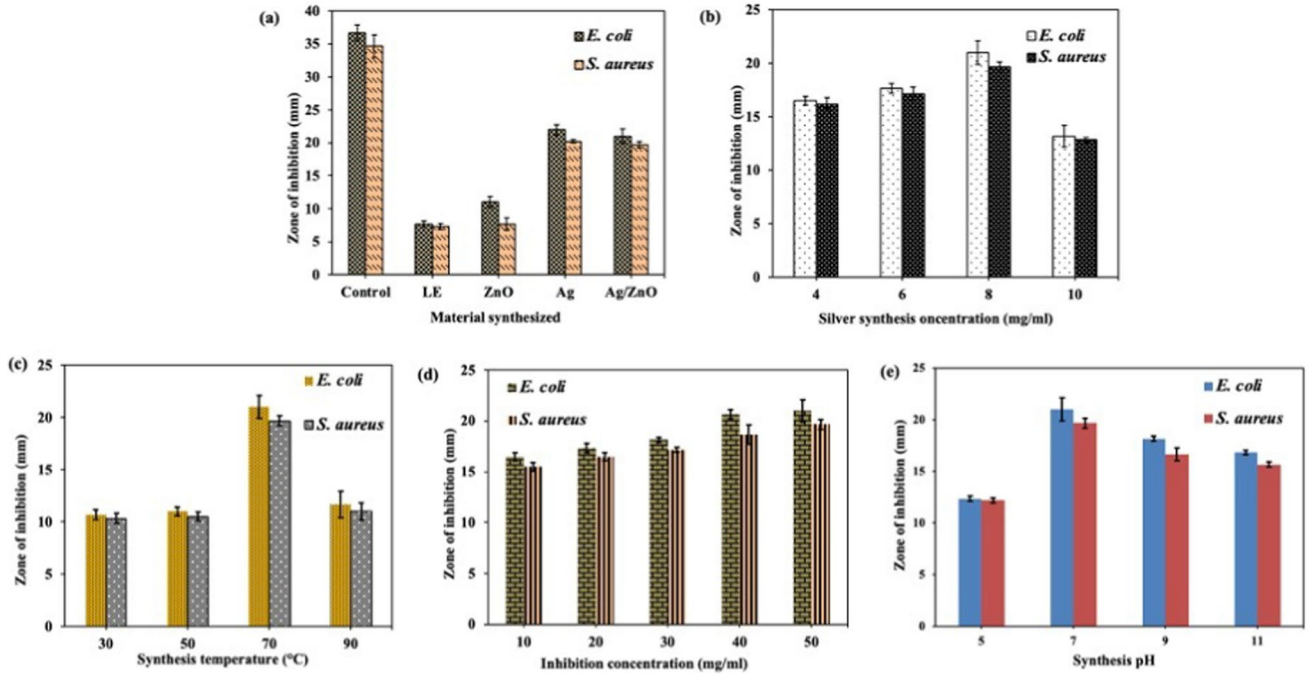

Fig. 7 Zone of inhibition for the synthesized nanoparticles on *E. coli* and *S. aureus* **a** pure Ag NPs, ZnO NPs, Ag–ZnO NCs, leaf extract and control **b** Ag–ZnO NCs at different Ag^+ synthesis concentration, **c** Ag–ZnO NPs at different synthesis temperature **d** Ag–ZnO NCs at different inhibitory concentration and **e** Ag–ZnO NCs at different pH

by the properties of the cell wall and membrane of the bacteria and the nature or properties of the NPs. Gram-negative bacteria have a thin peptidoglycan layer, compared to gram-positive bacteria which has thick and rigid peptidoglycan layer crosslinked by peptide chains. The thin layer of gram-negative bacteria facilitates easy penetration of the NPs to the bacterial nuclei, therefore, limiting cell regeneration [25, 86]. On the other hand, there is an electrostatic interaction between the positive NPs and the gram-negative bacterial membrane which is negatively charged. The attraction facilitates easy penetration of the NPs into the bacterial cell unlike gram-positive bacterial cells [87, 88]. The Ag–ZnO NCs were synthesized in four different temperatures, 30, 50, 70, and 90 °C to establish optimum conditions. According to the inhibition results, the highest inhibition was demonstrated by the NPs synthesized at 70 °C as indicated in Fig. 7c. Ag–ZnO NCs obtained above 70 °C had low microbial inhibition which might be attributed to the increased nucleation rate that leads to large particle size formation [36, 50]. The effect of silver doping concentration was also studied, and the increase in concentration increased the bacterial growth inhibition as demonstrated in Fig. 7b. This signifies that silver is a good antimicrobial agent [89, 90]. Figure 7d shows a positive correlation between the increased inhibition concentration from 10 to 50 mg and increased microbial inhibition for both strains as a result of increased dosage concentration of the nanoparticles per bacterial strain. The synthesis pH for Ag–ZnO NCs was also investigated and found to give the best inhibition results at pH 7 as indicated in Fig. 7e. These results correspond to the XRD results discussed above which shows at this pH the NPs have the smallest average size.

In this research, green synthesized nanomaterials have displayed exceptional effectiveness in inhibiting the growth of both gram-negative and gram-positive bacteria, surpassing previously reported research outcomes. These findings, highlighted in Table 1, reveal significantly lower minimum inhibition concentrations of the green synthesized nanoparticles, underscoring their potential to revolutionize antimicrobial strategies. This research not only showcases the promise of eco-friendly synthesis methods but also underscores their fundamental role in the development of highly potent antibacterial agents.

3.5 Antimicrobial mechanism

The antimicrobial mechanism of Ag–ZnO involves the synergistic action of silver (Ag) and zinc oxide (ZnO) nanoparticles. Ag possesses potent antimicrobial properties due to its ability to release silver ions (Ag^+) that can disrupt bacterial cell membranes and inhibit essential cellular functions resulting in the cellular death of affected bacteria [95, 96]. The Ag^+ binds to the thiol groups of proteins and enzymes, leading to the inhibition of enzyme activity and DNA replication. The formation of free Ag radical attacks the bacterial membrane lipids causing their dissociation, and damage, and finally inhibits the growth of the bacteria [97]. Additionally, Ag^+ can be internalized and generate reactive oxygen species (ROS), creating oxidative stress that alters the cell cycle and stimulates cell death through apoptosis or autophagy [77]. Furthermore, it is reported that Ag^+ binds to the sulfhydryl groups of the metabolic enzymes of the bacterial electron transport chain bringing about their inactivation [98]. On the other hand, ZnO nanoparticles exhibit antimicrobial activity by releasing Zn^{2+} ions that disrupt the integrity of bacterial membranes and interfere with intracellular processes [36, 91]. ZnO nanoparticles can also generate ROS, leading to oxidative stress and cellular damage. The combination of Ag and ZnO nanoparticles in Ag–ZnO nanocomposites enhances the antimicrobial activity by providing a dual mechanism of action, resulting in effective inhibition of various pathogens, including bacteria and fungi.

4 Conclusions

Ag–ZnO NCs were successfully synthesized using an environmentally friendly and efficient method by using *Launaea cornuta* leaf extract. The presence of phytochemical compounds in the leaf extract played a crucial role as reducing and capping agents during the synthesis process. The XRD, TEM, and SEM analyses confirmed the spherical and crystalline nature of the composites, with an average particle size of 21.5 nm under optimum conditions. The size and controlled agglomeration of the synthesized nanoparticles were influenced by the synthesis pH, temperature, and silver concentration. The antimicrobial efficacy of the Ag–ZnO NCs was assessed against *E. coli* and *S. aureus* bacterial strains, demonstrating significant inhibitory effects. Notably, the inhibitory activity was more pronounced against *E. coli* (gram-negative bacteria) compared to *S. aureus* (gram-positive bacteria). Thus, the *Launaea cornuta* leaf extract holds great promise as a potential source of phytochemical compounds for the synthesis of Ag–ZnO NCs, replacing synthetic chemicals. Furthermore, the incorporation of ZnO into Ag NPs has proven effective in controlling agglomeration, shape, and particle size, offering a sustainable approach to nanoparticle synthesis.

Table 1 Comparison of antimicrobial activity of Ag NPs, ZnO NPs and Ag–ZnO NCs of this study with other studies

Plant extract	Bacteria	Nanoparticles	Crystollite size (nm)	Concentration (MIC)	Zone of inhibition (mm)	References
Ocimum tenuiflorum seed extract	*Escherichia coli*	Ag–ZnO	54	2 mg/mL	Total inhibition in 15 min	[6]
Trigonella foenum-graecum leaf extract	*Staphylococcus aureus*	Ag–ZnO		20 mg/mL	13.5 ± 0.707	[91]
	Escherichia coli	Ag–ZnO		20 mg/mL	12.5 ± 0.707	[91]
Suaeda aegyptiaca leaf extract	*Staphylococcus aureus*	ZnO	60	10 mg/mL	16.01	[92]
Impatiens balsamina	*Staphylococcus aureus*	Ag	20.33	–	13.8	[1]
	Escherichia coli	Ag	20.33	–	8.9	[1]
Carica Papaya fruit	*Staphylococcus aureus*	Ag	75.68	169.9 ppm	11	[93]
	Escherichia coli	Ag	75.68	169.9 ppm	2	[93]
Launaea cornuta leaf extract	*Escherichia coli*	Ag	50.64	10 mg/ml	19.3 ± 0.94	This study
	Escherichia coli	ZnO	22.08		9.3 ± 0.83	
	Escherichia coli	Ag–ZnO	21.51		16.5 ± 0.46	
	Staphylococcus aureus	Ag	50.64		17.67 ± 0.96	
	Staphylococcus aureus	ZnO	22.08		6.5 ± 0.41	
	Staphylococcus aureus	Ag–ZnO	21.51		15.5 ± 0.56	
Aloe Socotrina leaf extract	*Escherichia coli*	ZnO	15–50	100 µg/mL	25 ± 1.7	[94]
Pistacia atlantica resin	*Staphylococcus aureus*	Ag–ZnO	18.9	0.0001 mg/mL	12 ± 0.06	[15]
	Escherichia coli	Ag–ZnO	18.9	0.0001 mg/mL	15.2 ± 0.007	[15]

Acknowledgements The authors acknowledge the African Development Bank through the Nelson Mandela African Institution of Science and Technology (NM-AIST) Grant ID 2100155032816 and the Queen Elizabeth Scholarship-Advanced Scholars program (QES-AS) through the Canadian Queen Elizabeth II Diamond Jubilee Scholarship program funded by Canada's International Development Research Centre [IDRC] for funding this study.

Author contributions EM: Conceptualization, methodology, formal analysis and investigation, writing—original draft preparation, visualization. SGM: Conceptualization, methodology, writing—review and editing. ODB: Conceptualization, methodology, writing-review and editing, supervision. MR: Conceptualization, methodology, writing—review and editing, supervision. RM: Conceptualization, methodology, writing—review and editing, supervision.

Data availability The datasets generated and/or analyzed in this study are available in the DRYAD repository and can be accessed through the following link: https://datadryad.org/stash/share/8_UpVqAbW6GsvrRsAznCeEYg65fu1iXAEwXJi-Zrtlw

Declarations

Competing interests The authors declare no competing interests.

References

1. Aritonang HF, Koleangan H, Wuntu AD. Synthesis of silver nanoparticles using aqueous extract of medicinal plants' (*Impatiens balsamina* and *Lantana camara*) fresh leaves and analysis of antimicrobial activity. Int J Microbiol. 2019;10:1–8. https://doi.org/10.1155/2019/8642303.
2. Sivagnanam SP, Getachew AT, Choi JH. Green synthesis of silver nanoparticles from deoiled brown algal extract via Box–Behnken based design and their antimicrobial and sensing properties. Green Process Synth. 2017;6:147–60. https://doi.org/10.1515/gps-2016-0052.
3. Gurunathan S, Kalishwaralal K, Vaidyanathan R, Venkataraman D, Pandian SRK, Muniyandi J, et al. Biosynthesis, purification and characterization of silver nanoparticles using *Escherichia coli*. Colloids Surf B Biointerfaces. 2009;74:328–35. https://doi.org/10.1016/j.colsurfb.2009.07.048.
4. Khodashenas B, Ghorbani HR. Synthesis of silver nanoparticles with different shapes. Arab J Chem. 2019;12:1823–38. https://doi.org/10.1016/j.arabjc.2014.12.014.
5. Ratan ZA, Haidere MF, Nurunnabi M, Shahriar SM, Ahammad AJS, Shim YY, et al. Green chemistry synthesis of silver nanoparticles and their potential anticancer effects. Cancers (Basel). 2020;12:855–80. https://doi.org/10.3390/cancers12040855.
6. Panchal P, Paul DR, Sharma A, Choudhary P, Meena P, Nehra SP. Biogenic mediated Ag/ZnO nanocomposites for photocatalytic and antibacterial activities towards disinfection of water. J Colloid Interface Sci. 2020;563:370–80. https://doi.org/10.1016/j.jcis.2019.12.079.
7. Dawadi S, Katuwal S, Gupta A, Lamichhane U, Thapa R, Jaisi S, et al. Current research on silver nanoparticles: synthesis, characterization, and applications. J Nanomater. 2021. https://doi.org/10.1155/2021/6687290.
8. Rajeshkumar S, Yadav K, Sridharan M, Roopan SM. Nano silver: an overview of shape, size-controlled synthesis and their antibacterial property. High Energy Chem. 2023;57:205–16. https://doi.org/10.1134/S001814392303013X.
9. Roberson M, Rangari V, Jeelani S, Samuel T, Yates C. Synthesis and characterization silver, zinc oxide and hybrid silver/zinc oxide nanoparticles for antimicrobial applications nano. Life. 2014;04:1440003. https://doi.org/10.1142/s1793984414400030.
10. Gurgur E, Oluyamo SS, Omotunde AO, Adetuyi OI. Green synthesis of zinc oxide nanoparticles and zinc oxide—silver, zinc oxide–copper nanocomposites using *Bridelia ferruginea* as biotemplate. SN Appl Sci. 2020;2:1–12. https://doi.org/10.1007/s42452-020-2269-3.
11. Alam F, Balani K. Role of silver/zinc oxide in affecting de-adhesion strength of *Staphylococcus aureus* on polymer biocomposites. Mater Sci Eng C. 2017;75:1106–14. https://doi.org/10.1016/j.msec.2017.02.131.
12. Lee J. Silver nanoparticles synthesized from *Adenium obesum* leaf extract induced DNA damage, apoptosis and autophagy via generation of reactive oxygen species. Colloids Surf B Biointerfaces. 2016;141:158–69. https://doi.org/10.1016/j.colsurfb.2016.01.027.

13. Kumar TP, Triveni RM, Sangeetha P, Sakthivel P, Revathi SK, Kumar AS, et al. Highly efficient performance of activated carbon impregnated with Ag, ZnO and Ag/ZnO nanoparticles as antimicrobial materials. In: AIChE annual meeting, conference proceedings, vol. 2019–November, American Institute of Chemical Engineers. 2015;130:108034–43. https://doi.org/10.1039/x0xx00000x
14. Pirtarighat S, Ghannadnia M, Baghshahi S. Green synthesis of silver nanoparticles using the plant extract of *Salvia spinosa* grown in vitro and their antibacterial activity assessment. J Nanostruct Chem. 2019;9:1–9. https://doi.org/10.1007/s40097-018-0291-4.
15. Jomehzadeh N, Koolivand Z, Dahdouh E, Akbari A, Zahedi A. Investigating in-vitro antimicrobial activity, biosynthesis, and characterization of silver nanoparticles, zinc oxide nanoparticles, and silver-zinc oxide nanocomposites using *Pistacia atlantica* Resin. Mater Today Commun. 2021;27:102457. https://doi.org/10.1016/j.mtcomm.2021.102457.
16. Babu AT, Antony R. Green synthesis of silver doped nano metal oxides of zinc & copper for antibacterial properties, adsorption, catalytic hydrogenation & photodegradation of aromatics. J Environ Chem Eng. 2019;7:102840–79. https://doi.org/10.1016/j.jece.2018.102840.
17. Patil SS, Mali MG, Tamboli MS, Patil DR, Kulkarni MV, Yoon H, et al. Green approach for hierarchical nanostructured Ag–ZnO and their photocatalytic performance under sunlight. Catal Today. 2016;260:126–34. https://doi.org/10.1016/j.cattod.2015.06.004.
18. Shreema K, Mathammal R, Kalaiselvi V, Vijayakumar S, Selvakumar K, Senthil K. Green synthesis of silver doped zinc oxide nanoparticles using fresh leaf extract *Morinda citrifoliaand* its antioxidant potential. Mater Today Proc. 2021;47:2126–31. https://doi.org/10.1016/j.matpr.2021.04.627.
19. Rajeshkumar S, Nandhini NT, Manjunath K, Sivaperumal P, Krishna Prasad G, Alotaibi SS, et al. Environment friendly synthesis copper oxide nanoparticles and its antioxidant, antibacterial activities using Seaweed (*Sargassum longifolium*) extract. J Mol Struct. 2021. https://doi.org/10.1016/j.molstruc.2021.130724.
20. Roopan SM, Khan FRN. ZnO nanorods catalyzed N-alkylation of piperidin-4-one, 4(3H)-pyrimidone, and ethyl 6-chloro-1,2-dihydro-2-oxo-4-phenylquinoline-3-carboxylate. Chem Pap. 2010;64:678–82. https://doi.org/10.2478/s11696-010-0045-3.
21. Surendra TV, Roopan SM, Al-Dhabi NA, Arasu MV, Sarkar G, Suthindhiran K. Vegetable peel waste for the production of ZnO nanoparticles and its toxicological efficiency, antifungal, hemolytic, and antibacterial activities. Nanoscale Res Lett. 2016. https://doi.org/10.1186/s11671-016-1750-9.
22. Madhumitha G, Elango G, Roopan SM. Biotechnological aspects of ZnO nanoparticles: overview on synthesis and its applications. Appl Microbiol Biotechnol. 2016;100:571–81. https://doi.org/10.1007/s00253-015-7108-x.
23. Saha R, Subramani K, Petchi Muthu Raju SAK, Rangaraj S, Venkatachalam R. *Psidium guajava* leaf extract-mediated synthesis of ZnO nanoparticles under different processing parameters for hydrophobic and antibacterial finishing over cotton fabrics. Prog Org Coat. 2018;124:80–91. https://doi.org/10.1016/j.porgcoat.2018.08.004.
24. Moradi M, Haghighi M, Allahyari S. Precipitation dispersion of Ag–ZnO nanocatalyst over functionalized multiwall carbon nanotube used in degradation of acid orange from wastewater. Process Saf Environ Prot. 2017;107:414–27. https://doi.org/10.1016/j.psep.2017.03.010.
25. Mtavangu SG, Machunda RL, van der Bruggen B, Njau KN. In situ facile green synthesis of Ag–ZnO nanocomposites using *Tetradenia riperia* leaf extract and its antimicrobial efficacy on water disinfection. Sci Rep. 2022;12:15359–72. https://doi.org/10.1038/s41598-022-19403-1.
26. Dias HB, Bernardi MIB, Marangoni VS, de Abreu Bernardi AC, de Souza Rastelli AN, Hernandes AC. Synthesis, characterization and application of Ag doped ZnO nanoparticles in a composite resin. Mater Sci Eng C. 2019;96:391–401. https://doi.org/10.1016/j.msec.2018.10.063.
27. Hasell T, Yang J, Wang W, Brown PD, Howdle SM. A facile synthetic route to aqueous dispersions of silver nanoparticles. Mater Lett. 2007;61:4906–10. https://doi.org/10.1016/j.matlet.2007.03.072.
28. Sharma VK, Yngard RA, Lin Y. Silver nanoparticles: green synthesis and their antimicrobial activities. Adv Colloid Interface Sci. 2009;145:83–96. https://doi.org/10.1016/j.cis.2008.09.002.
29. Akintelu SA, Folorunso AS. A review on green synthesis of zinc oxide nanoparticles using plant extracts and its biomedical applications. Bionanoscience. 2020;10:848–63. https://doi.org/10.1007/s12668-020-00774-6.
30. Zeghoud S, Hemmami H, Ben Seghir B, Ben Amor I, Kouadri I, Rebiai A, et al. A review on biogenic green synthesis of ZnO nanoparticles by plant biomass and their applications. Mater Today Commun. 2022;33:104747–56. https://doi.org/10.1016/j.mtcomm.2022.104747.
31. Krasner SW, Weinberg HS, Richardson SD, Pastor SJ, Chinn R, Sclimenti MJ, et al. Occurrence of a new generation of disinfection byproducts. Environ Sci Technol. 2006;40:7175–85. https://doi.org/10.1021/es060353j.
32. Zhao Y, Anichina J, Lu X, Bull RJ, Krasner SW, Hrudey SE, et al. Occurrence and formation of chloro- and bromo-benzoquinones during drinking water disinfection. Water Res. 2012;46:4351–60. https://doi.org/10.1016/j.watres.2012.05.032.
33. Masum MI, Siddiqa MM, Ali KA, Zhang Y, Abdallah Y, Ibrahim E, et al. Biogenic synthesis of silver nanoparticles using *Phyllanthus emblica-fruit* extract and its inhibitory action against the pathogen acidovorax oryzaestrain RS-2 of rice bacterial brown stripe. Front Microbiol. 2019;10:820–37. https://doi.org/10.3389/fmicb.2019.00820.
34. Priya, Naveen, Kaur K, Sidhu AK. Green synthesis: an eco-friendly route for the synthesis of iron oxide nanoparticles. Front Nanotechnol. 2021;3:655062–77. https://doi.org/10.3389/fnano.2021.655062.
35. Jadoun S, Arif R, Jangid NK, Meena RK. Green synthesis of nanoparticles using plant extracts: a review. Environ Chem Lett. 2021;19:355–74. https://doi.org/10.1007/s10311-020-01074-x.
36. Bala N, Saha S, Chakraborty M, Maiti M, Das S, Basu R, et al. Green synthesis of zinc oxide nanoparticles using *Hibiscus subdariffa* leaf extract: effect of temperature on synthesis, anti-bacterial activity and anti-diabetic activity. RSC Adv. 2015;5:4993–5003. https://doi.org/10.1039/c4ra12784f.
37. Kharissova O, Dias HVR, Kharisov BI, Pérez BO, Pérez VMJ. The greener synthesis of nanoparticles. Trends Biotechnol. 2013;31:240–8. https://doi.org/10.1016/j.tibtech.2013.01.003.
38. Gour A, Jain NK. Advances in green synthesis of nanoparticles. Artif Cells Nanomed Biotechnol. 2019;47:844–51. https://doi.org/10.1080/21691401.2019.1577878.
39. Fayaz H, Karthik K, Christiyan KGJ, Kumar MA, Sivakumar A, Kaliappan S, et al. An investigation on the activation energy and thermal degradation of biocomposites of Jute/Bagasse/Coir/nano TiO_2/epoxy-reinforced polyaramid fibers. J Nanomater. 2022. https://doi.org/10.1155/2022/3758212.
40. Karthik K, Rajamani D, Venkatesan EP, Shajahan MI, Rajhi AA, Aabid A, et al. Experimental investigation of the mechanical properties of carbon/basalt/SiC nanoparticle/polyester hybrid composite materials. Crystals (Basel). 2023. https://doi.org/10.3390/cryst13030415.

41. Khalil MMH, Ismail EH, El-Baghdady KZ, Mohamed D. Green synthesis of silver nanoparticles using olive leaf extract and its antibacterial activity. Arab J Chem. 2014;7:1131–9. https://doi.org/10.1016/j.arabjc.2013.04.007.
42. Mortezagholi B, Movahed E, Fathi A, Soleimani M, Forutan Mirhosseini A, Zeini N, et al. Plant-mediated synthesis of silver-doped zinc oxide nanoparticles and evaluation of their antimicrobial activity against bacteria cause tooth decay. Microsc Res Tech. 2022;85:3553–64. https://doi.org/10.1002/jemt.24207.
43. Mohamad NAN, Arham NA, Jai J, Hadi A. Plant extract as reducing agent in synthesis of metallic nanoparticles: a review. Adv Mat Res. 2014;832:350–5. https://doi.org/10.4028/www.scientific.net/AMR.832.350.
44. Kuppusamy P, Yusoff MM, Maniam GP, Govindan N. Biosynthesis of metallic nanoparticles using plant derivatives and their new avenues in pharmacological applications: an updated report. Saudi Pharm J. 2016;24:473–84. https://doi.org/10.1016/j.jsps.2014.11.013.
45. Ramesh V, Karthik K, Cep R, Elangovan M. Influence of stacking sequence on mechanical properties of basalt/ramie biodegradable hybrid polymer composites. Polymers (Basel). 2023. https://doi.org/10.3390/polym15040985.
46. Hussain I, Singh NB, Singh A, Singh H, Singh SC. Green synthesis of nanoparticles and its potential application. Biotechnol Lett. 2016;38:545–60. https://doi.org/10.1007/s10529-015-2026-7.
47. Guzmán MG, Dille J, Godet S. Synthesis of silver nanoparticles by chemical reduction method and their antibacterial activity. Int J Chem Biomol Eng. 2009;2:104–7.
48. Yong J, Beom SÆ, Kim S. Rapid biological synthesis of silver nanoparticles using plant leaf extracts. Bioprocess Biosyst Eng. 2009;32:79–84. https://doi.org/10.1007/s00449-008-0224-6.
49. Ahmad S, Munir S, Zeb N, Ullah A, Khan B, Ali J, et al. Green nanotechnology: a review on green synthesis of silver nanoparticles—an ecofriendly approach. Int J Nanomed. 2019;14:5087–107. https://doi.org/10.2147/IJN.S200254.
50. Fayaz MA, Balaji K, Kalaichelvan PT, Venkatesan R. Fungal based synthesis of silver nanoparticles: an effect of temperature on the size of particles. Colloids Surf B Biointerfaces. 2009;74:123–6. https://doi.org/10.1016/j.colsurfb.2009.07.002.
51. Indriyani A, Yulizar Y, Tri Yunarti R, Oky Bagus Apriandanu D, Marcony Surya R. One-pot green fabrication of $BiFeO_3$ nanoparticles via *Abelmoschus esculentus* L. leaves extracts for photocatalytic dye degradation. Appl Surf Sci. 2021;563:150113–25. https://doi.org/10.1016/j.apsusc.2021.150113.
52. Surya MR, Mauliddiyah S, Apriandanu DOB, Sudirman, Yulizar Y. $SmMnO_3$-decorated ZnO in a hexane-water interface for enhancing visible light-driven photocatalytic degradation of malachite green. Chemosphere. 2022;304:135125. https://doi.org/10.1016/j.chemosphere.2022.135125.
53. Balogun ST, Stephenson C, Akanmu AO, Gamache S, Jibrin J. Antipseudomonal activity of aqueous and methanolic leaf extracts of *Lactuca serriola* Linn. (Astereceae). J Chem Chem Eng. 2017;8:157–62.
54. Awan AF, Akhtar MS, Anjum I, Mushtaq MN, Almas F, Mannan A, et al. Anti-oxidant and hepatoprotective effects of *Lactuca serriola* and its phytochemical screening by HPLC and FTIR analysis. Pak J Pharm Sci. 2020;33:2823–30. https://doi.org/10.36721/PJPS.2020.33.6.SUP.2823-2830.1.
55. Muriira Karau G, Nyagah E, Njagi M, King'ori Machocho A, Koech LC, Wangai LN, et al. Profiling of the chemical compounds in ethyl acetate extracts of *Launaea cornuta* asteraceae by GC–MS. Int J Pharmacogn. 2014;1:296–300. https://doi.org/10.13040/IJPSR.0975-8232.IJP.1(5).296-00.
56. Akimat EK, Omwenga GI, Moriasi GA, Ngugi MP. Antioxidant, anti-inflammatory, acute oral toxicity, and qualitative phytochemistry of the aqueous root extract of *Launaea cornuta* (Hochst. Ex. Oliv. & Hiern.). J Evid Based Integr Med. 2021. https://doi.org/10.1177/2515690X211064585.
57. Misonge JO, Kinyanjui JG, Kingori WM, Mwalukumbi JM. Phytochemical screening and cytotoxicity evaluation of *Launaea cornuta* H. (Asteraceae) using brine shrimp. Merit Res J Med Med Sci. 2015;3:116–20.
58. Roopan SM, Mathew RS, Mahesh SS, Titus D, Aggarwal K, Bhatia N, et al. Environmental friendly synthesis of zinc oxide nanoparticles and estimation of its larvicidal activity against *Aedes aegypti*. Int J Environ Sci Technol. 2019;16:8053–60. https://doi.org/10.1007/s13762-018-2175-z.
59. Ashraf H, Anjum T, Riaz S, Naseem S. Microwave-assisted green synthesis and characterization of silver nanoparticles using *Melia azedarach* for the management of fusarium wilt in tomato. Front Microbiol. 2020;11:238–59. https://doi.org/10.3389/fmicb.2020.00238.
60. Mehta BK, Chhajlani M, Shrivastava BD. Green synthesis of silver nanoparticles and their characterization by XRD. J Phys Conf Ser. 2017;836:012050–4. https://doi.org/10.1088/1742-6596/836/1/012050.
61. Marimuthu T, Anandhan N, Mahalingam T, Thangamuthu R, Mummoorthi M. Effect of *P. murex* on the properties of spin coated ZnO thin films for dye sensitized solar cell applications. J Mater Sci Mater Electron. 2015;26:7577–87. https://doi.org/10.1007/s10854-015-3394-4.
62. Ifijen IH, Maliki M, Anegbe B. Synthesis, photocatalytic degradation and antibacterial properties of selenium or silver doped zinc oxide nanoparticles: a detailed review. OpenNano. 2022;8:100082–106. https://doi.org/10.1016/j.onano.2022.100082.
63. Liu Z, Wang Y, Zu Y, Fu Y, Li N, Guo N, et al. Synthesis of polyethylenimine (PEI) functionalized silver nanoparticles by a hydrothermal method and their antibacterial activity study. Mater Sci Eng C. 2014;42:31–7. https://doi.org/10.1016/j.msec.2014.05.007.
64. Ramesh PS, Kokila T, Geetha D. Plant mediated green synthesis and antibacterial activity of silver nanoparticles using Emblica officinalis fruit extract. Spectrochim Acta A Mol Biomol Spectrosc. 2015;142:339–43. https://doi.org/10.1016/j.saa.2015.01.062.
65. Hemmati S, Rashtiani A, Zangeneh MM, Mohammadi P, Zangeneh A, Veisi H. Green synthesis and characterization of silver nanoparticles using Fritillaria flower extract and their antibacterial activity against some human pathogens. Polyhedron. 2019;158:8–14. https://doi.org/10.1016/j.poly.2018.10.049.
66. Yulizar Y, Gunlazuardi J, Apriandanu DOB, Syahfitri TWW. CuO-modified $CoTiO_3$ via *Catharanthus roseus* extract: a novel nanocomposite with high photocatalytic activity. Mater Lett. 2020;277:128349–53. https://doi.org/10.1016/j.matlet.2020.128349.
67. Suwarno AC, Yulizar Y, Apriandanu DOB, Surya RM. Biosynthesis of Dy_2O_3 nanoparticles using *Piper retrofractum* Vahl extract: optical, structural, morphological, and photocatalytic properties. J Mol Struct. 2022;1264:133123–32. https://doi.org/10.1016/j.molstruc.2022.133123.
68. Wang YY, Li JQ, Liu HG, Wang YZ. Attenuated total reflection-Fourier transform infrared spectroscopy (ATR-FTIR) combined with chemometrics methods for the classification of Lingzhi species. Molecules. 2019;24:2210–22. https://doi.org/10.3390/molecules24122210.

69. Yulizar Y, Eprasatya A, Bagus Apriandanu DO, Yunarti RT. Facile synthesis of ZnO/$GdCoO_3$ nanocomposites, characterization and their photocatalytic activity under visible light illumination. Vacuum. 2021;183:109821. https://doi.org/10.1016/j.vacuum.2020.109821.
70. Elviera, Yulizar Y, Apriandanu DOB, Marcony Surya R. Fabrication of novel $SnWO_4$/ZnO using *Muntingia calabura* L. leaf extract with enhanced photocatalytic methylene blue degradation under visible light irradiation. Ceram Int. 2022;48:3564–77. https://doi.org/10.1016/j.ceramint.2021.10.135.
71. Ankamwar B. Biosynthesis of gold nanoparticles (Green-Gold) using leaf extract of *Terminalia catappa*. E-J Chem. 2010;7:1334–9. https://doi.org/10.1155/2010/745120.
72. Khalil MMH, Ismail EH, El-Magdoub F. Biosynthesis of Au nanoparticles using olive leaf extract. 1st nano updates. Arab J Chem. 2012;5:431–7. https://doi.org/10.1016/j.arabjc.2010.11.011.
73. Alnehia A, Al-Sharabi A, Al-Hammadi AH, Al-Odayni AB, Alramadhan SA, Alodeni RM. Phyto-mediated synthesis of silver-doped zinc oxide nanoparticles from *Plectranthus barbatus* leaf extract: optical, morphological, and antibacterial properties. Biomass Convers Biorefin. 2023. https://doi.org/10.1007/s13399-023-03907-5.
74. Naseer M, Aslam U, Khalid B, Chen B. Green route to synthesize zinc oxide nanoparticles using leaf extracts of *Cassia fistula* and *Melia azadarach* and their antibacterial potential. Sci Rep. 2020;10:9055. https://doi.org/10.1038/s41598-020-65949-3.
75. Kumar P, Selvi SS, Govindaraju M. Seaweed-mediated biosynthesis of silver nanoparticles using *Gracilaria corticata* for its antifungal activity against *Candida* spp. Appl Nanosci (Switzerland). 2013;3:495–500. https://doi.org/10.1007/s13204-012-0151-3.
76. Singh K, Singh J, Rawat M. Green synthesis of zinc oxide nanoparticles using *Punica granatum* leaf extract and its application towards photocatalytic degradation of Coomassie brilliant blue R-250 dye. SN Appl Sci. 2019;1:624–31. https://doi.org/10.1007/s42452-019-0610-5.
77. Guilger-Casagrande M, de Lima R. Synthesis of silver nanoparticles mediated by fungi: a review. Front Bioeng Biotechnol. 2019;7:287–302. https://doi.org/10.3389/fbioe.2019.00287.
78. Yusof HM, Mohamad R, Zaidan UH, Rahman NAA. Microbial synthesis of zinc oxide nanoparticles and their potential application as an antimicrobial agent and a feed supplement in animal industry: a review. J Anim Sci Biotechnol. 2019. https://doi.org/10.1186/s40104-019-0368-z.
79. Sathyavathi R, Krishna MB, Rao SV, Saritha R, Rao DN. Biosynthesis of silver nanoparticles using *Coriandrum sativum* leaf extract and their application in nonlinear optics. Adv Sci Lett. 2010;3:138–43. https://doi.org/10.1166/asl.2010.1099.
80. Alharthi FA, Alghamdi AA, Al-Zaqri N, Alanazi HS, Alsyahi AA, El MA, et al. Facile one-pot green synthesis of Ag–ZnO Nanocomposites using potato peeland their Ag concentration dependent photocatalytic properties. Sci Rep. 2020;10:1–14. https://doi.org/10.1038/s41598-020-77426-y.
81. Chithra MJ, Pushpanathan MSK. Effect of pH on crystal size and photoluminescence property of ZnO nanoparticles prepared by chemical precipitation method. Acta Metall Sin (Engl Lett). 2015;28:394–404. https://doi.org/10.1007/s40195-015-0218-8.
82. Venis RA, Basu OD. Mechanisms and efficacy of disinfection in ceramic water filters: a critical review. Crit Rev Environ Sci Technol. 2021;51:2934–74. https://doi.org/10.1080/10643389.2020.1806685.
83. Ghosh T, Das AB, Jena B, Pradhan C. Frontiers in life science antimicrobial effect of silver zinc oxide (Ag–ZnO) nanocomposite particles. Front Life Sci. 2015;8:47–54. https://doi.org/10.1080/21553769.2014.952048.
84. Talari MK, Bakar A, Majeed A, Tripathi DK, Tripathy M. Synthesis, characterization and antimicrobial investigation of mechanochemically processed silver doped ZnO nanoparticles. Chem Pharm Bull. 2012;60(7):818–24. https://doi.org/10.1248/cpb.c110479.
85. Cardoza-Contreras MN, Vásquez-Gallegos A, Vidal-Limon A, Romo-Herrera JM, Águila S, Contreras OE. Photocatalytic and antimicrobial properties of Ga doped and Ag doped ZnO nanorods for water treatment. Catalysts. 2019;9:165–76. https://doi.org/10.3390/catal9020165.
86. Mousavi-kouhi SM, Beyk-khormizi A, Sadegh M. Silver-zinc oxide nanocomposite: from synthesis to antimicrobial and anticancer properties. Ceram Int. 2021;47:21490–7. https://doi.org/10.1016/j.ceramint.2021.04.160.
87. Sondi I, Salopek-Sondi B. Silver nanoparticles as antimicrobial agent: a case study on *E. coli* as a model for Gram-negative bacteria. J Colloid Interface Sci. 2004;275(177):182. https://doi.org/10.1016/j.jcis.2004.02.012.
88. Pazos-Ortiz E, Roque-Ruiz JH, Hinojos-Márquez EA, López-Esparza J, Donohué-Cornejo A, Cuevas-González JC, et al. Dose-dependent antimicrobial activity of silver nanoparticles on polycaprolactone fibers against gram-positive and gram-negative bacteria. J Nanomater. 2017. https://doi.org/10.1155/2017/4752314.
89. Lalley J, Dionysiou DD, Varma RS, Shankara S, Yang DJ, Nadagouda MN. ScienceDirect Silver-based antibacterial surfaces for drinking water disinfection—an overview. Curr Opin Chem Eng. 2014;3:25–9. https://doi.org/10.1016/j.coche.2013.09.004.
90. Choi O, Deng KK, Kim NJ, Ross L, Surampalli RY, Hu Z. The inhibitory effects of silver nanoparticles, silver ions, and silver chloride colloids on microbial growth. Water Res. 2008;42:3066–74. https://doi.org/10.1016/j.watres.2008.02.021.
91. Fahimmunisha BA, Ishwarya R, AlSalhi MS, Devanesan S, Govindarajan M, Vaseeharan B. Green fabrication, characterization and antibacterial potential of zinc oxide nanoparticles using *Aloe socotrina* leaf extract: a novel drug delivery approach. J Drug Deliv Sci Technol. 2020. https://doi.org/10.1016/j.jddst.2019.101465.
92. Noohpisheh Z, Amiri H, Farhadi S, Mohammadi-gholami A. Green synthesis of Ag–ZnO nanocomposites using *Trigonella foenum*-graecum leaf extract and their antibacterial, antifungal, antioxidant and photocatalytic properties. Spectrochim Acta A Mol Biomol Spectrosc. 2020;240:118595. https://doi.org/10.1016/j.saa.2020.118595.
93. Rajabi HR, Naghiha R, Kheirizadeh M, Sadatfaraji H, Mirzaei A, Alvand ZM. Microwave assisted extraction as an efficient approach for biosynthesis of zinc oxide nanoparticles: synthesis, characterization, and biological properties. Mater Sci Eng C. 2017;78:1109–18. https://doi.org/10.1016/j.msec.2017.03.090.
94. Mohammed MT, Farhan A, Abdula A. Green synthesis of silver nanoparticles using *Carica papaya* juice and study of their biochemical application. J Pharm Sci Res. 2019;11:1025–34.
95. Dibrov P, Dzioba J, Gosink KK, Häse CC. Chemiosmotic mechanism of antimicrobial activity of Ag^+ in Vibrio cholerae. Antimicrob Agents Chemother. 2002;46:2668–70. https://doi.org/10.1128/AAC.46.8.2668-2670.2002.
96. Hamouda T, Myc A, Donovan B, Shih AY, Reuter JD, Baker JR. A novel surfactant nanoemulsion with a unique non-irritant topical antimicrobial activity against bacteria, enveloped viruses and fungi. Microbiol Res. 2001;156:1–7. https://doi.org/10.1078/0944-5013-00069.

97. Siddiqi KS, Husen A, Rao RAK. A review on biosynthesis of silver nanoparticles and their biocidal properties. J Nanobiotechnology. 2018;16:14–42. https://doi.org/10.1186/s12951-018-0334-5.
98. Nakhjavani M, Nikkhah V, Sarafraz MM, Shoja S, Sarafraz M. Green synthesis of silver nanoparticles using green tea leaves: experimental study on the morphological, rheological and antibacterial behaviour. Heat Mass Trans. 2017;53:3201–9. https://doi.org/10.1007/s00231-017-2065-9.